chemosensors

MDPI

Article

Effects of Vacancy Defects and the Adsorption of Toxic Gas Molecules on Electronic, Magnetic, and Adsorptive Properties of g−ZnO: A First-Principles Study

Yang Shen [1,*], Zhihao Yuan [1], Zhen Cui [2,*], Deming Ma [1], Pei Yuan [1], Kunqi Yang [1], Yanbo Dong [1], Fangping Wang [1] and Enling Li [1,*]

[1] School of Science, Xi'an University of Technology, Xi'an 710054, China
[2] School of Automation and Information Engineering, Xi'an University of Technology, Xi'an 710048, China
* Correspondence: shenyang@xaut.edu.cn (Y.S.); zcui@xaut.edu.cn (Z.C.); lienling@xaut.edu.cn (E.L.)

Abstract: Using first principles based on density functional theory (DFT), the CO, NH_3, NO, and NO_2 gas adsorbed on intrinsic Graphite-like ZnO (g−ZnO) and vacancy-deficient g−ZnO were systematically studied. For intrinsic g−ZnO, the adsorption energy of NH_3, NO, and NO_2 adsorption defective g−ZnO systems increased significantly due to the introduction of Zn vacancy (V_{Zn}). Especially, for NH_3, NO, and NO_2 adsorbed Zn-vacancy g−ZnO (V_{Zn}/g−ZnO) systems increased to 1.366 eV, 2.540 eV and 2.532 eV, respectively. In addition, with the introduction of vacancies, the adsorption height of the gases adsorbed on V_{Zn}/g−ZnO system is significantly reduced, especially the adsorption height of the NH_3 adsorbed on V_{Zn}/g−ZnO system is reduced to 0.686 Å. It is worth mentioning that the introduction of O-vacancy (V_O) significantly enhances the charge transfer between NO or NO_2 and V_O/g−ZnO. This suggest that the defective g−ZnO is more suitable for detecting NH_3, NO and NO_2 gas. It is interesting to note that the adsorption of NO and NO_2 gases gives rise to magnetic moments of 1 μ_B and 0.858 μ_B for g−ZnO, and 1 μ_B and 1 μ_B for V_O/g−ZnO. In addition, V_{Zn} induced 1.996 μ_B magnetic moments for intrinsic g−ZnO, and the CO, NH_3, NO and NO_2 change the magnetic of V_{Zn}/g−ZnO. The adsorption of NO_2 causes the intrinsic g−ZnO to exhibit metallic properties, while the adsorption of NH_3 gas molecules causes V_{Zn}/g−ZnO also to show metallic properties. The adsorption of NO and NO_2 causes V_{Zn}/g−ZnO to display semi-metallic properties. These results facilitate the enrichment of defect detection means and the design of gas detection devices.

Keywords: g−ZnO; vacancy defect; adsorption; gas detection; magnetism

Citation: Shen, Y.; Yuan, Z.; Cui, Z.; Ma, D.; Yuan, P.; Yang, K.; Dong, Y.; Wang, F.; Li, E. Effects of Vacancy Defects and the Adsorption of Toxic Gas Molecules on Electronic, Magnetic, and Adsorptive Properties of g−ZnO: A First-Principles Study. *Chemosensors* **2023**, *11*, 38. https://doi.org/10.3390/chemosensors11010038

Academic Editors: Estefanía Núñez Carmona and Veronica Sberveglieri

Received: 25 November 2022
Revised: 23 December 2022
Accepted: 28 December 2022
Published: 2 January 2023

1. Introduction

Zinc Oxide (ZnO) has various dimensional anamorphs, such as zero-dimensional nanocrystals [1], one-dimensional nanowires [2], and two-dimensional (2D) nanofilms [3,4], which has a direct bandgap with the value of 3.37 eV [5,6]. In particular, 2D ZnO possesses high chemical or thermal stability [7–9], which is essential in the fields of gas detector devices [10,11], high-efficiency UV laser emitter devices at room temperature [12,13], etc. Therefore, 2D ZnO is rapidly becoming a recent research hotspot [14].

After Claeyssens et al. [15] revealed that graphene-like ZnO (g−ZnO) has a stable structure through theoretical calculation, Tusche et al. [8] experimentally verified that ZnO with a fibrillated ZnO structure could be converted to g−ZnO with a stable structure when the thickness is small enough (A few atoms). Sahoo et al. [16] synthesized planar 2D ZnO by hydrothermal method and revealed the formation of a 2D honeycomb lattice and the aggregated structure of layered ZnO. Altuntasoglu et al. [17] successfully prepared ZnO nanosheets by delamination of layered ZnO films. Qin et al. [18] prepared $LaCoO_3$ modified ZnO nanosheet materials with great improvement in gas sensitivity. Shen et al. [19] recently prepared ZnO and carbon materials composite aerogels for enhancing the photocatalytic

properties of ZnO. Shishiyanu et al. [20] prepared Sn-doped ZnO films, and they found good selectivity for NO_2 gas.

In addition, theoretical research on g−ZnO modification is also developing speedily. Cui et al. [21] covered that the formation of MoSSe/ZnO heterojunction structure changes the optical absorption properties of g−ZnO. Wang et al. [22] found that MoS_2/ZnO vdW heterostructure has application potential in photovoltaic and photocatalytic devices. Shen et al. [23] found that molecular doping (organic molecules) could achieve effective p-type doping. Guo et al. [24] found that the adjustable magnetic and electronic properties of monolayer ZnO can be achieved by nonmetallic doping. Theoretical studies to improve the gas detection performance of g−ZnO have also been widely followed by scholars. Meng et al. [5] investigated graphene (MoS_2) as a heterogeneous layer material stacked with g−ZnO to enhance interaction with NH_3 gas, and found that g−ZnO and its homogeneous and heterogeneous bilayer structures could be a candidate for gas-sensitive materials. However, there have been relatively few studies on g−ZnO and vacancy defective g−ZnO modifications for adsorption and detection of toxic gases [25].

Here, the gas molecules (CO, NH_3, NO, and NO_2) adsorbed on intrinsic g−ZnO and vacancy g−ZnO were systematically researched. The influence of defects on the interaction between g−ZnO and gas molecules and on the electronic properties is revealed by the adsorption energy, adsorption height, charge density difference (CDD), band structure, the density of states (DOS) and spin density (magnetic system) of the system, and the origin of the magnetism is also demonstrated. Our results provide theoretical guidance for the design of gas detection devices.

2. Computation Methods and Models

Using the Vienna ab initio simulation package (VASP) [26] to research the adsorption behavior of gas (CO, NH_3, NO, and NO_2) on intrinsic and defective g−ZnO. Electron exchange and correlation are achieved by the Perdew-Burke-Ernzernhof (PBE) function [27], while electron-ion interactions use the projection-enhanced wave method [28]. The DFT-3 method describes weak dispersion forces between layers [29,30]. The truncation energy of the plane wave is set to 500 eV [31]. The Brillouin zone is described by $3 \times 3 \times 1$ K-points centered on Γ point. The vacuum layer of 20 Å is set to avoid interactions between periodic structures [32,33]. Additionally, the data export and processing are realized by the VASPKIT code [34].

In addition, the adsorption energy is calculated as follows [35,36]:

$$E_{ad} = E_{total} - E_{I/D\text{-}g\text{-}ZnO} - E_G \quad (1)$$

where E_{ad} is the adsorption energy, E_{total} and E_G represent the energy of the adsorption system and gas, respectively. $E_{I/D\text{-}g-ZnO}$ represents the energy of intrinsic g−ZnO or defective g−ZnO. CDD can describe the distribution of charge transfer between gas and intrinsic or vacancy g−ZnO, and is calculated by [37]:

$$\Delta\rho = \rho_{total} - \rho_{I/D\text{-}g\text{-}ZnO} - \rho_G \quad (2)$$

where ρ_{total} and ρ_G represent the charge density (CD) of the adsorbed system and gas, respectively. $\rho_{I/D\text{-}g-ZnO}$ represents the CD of intrinsic g−ZnO or defective g−ZnO. The spin density is calculated as follows [38,39]:

$$\rho = \rho_{spin\text{-}up} - \rho_{spin\text{-}down} \quad (3)$$

where $\rho_{spin\text{-}up}$ and $\rho_{spin\text{-}down}$ represent the spin up and down of the magnetic systems, respectively.

The $4 \times 4 \times 1$ supercells are studied both intrinsic g−ZnO and defective g−ZnO. The difference is that defective g−ZnO has a Zinc vacancy (V_{Zn}) or Oxygen vacancy (V_O). All

atoms are entirely relaxed until the Hellmann-Feynman force is less than 10^{-2} eV $Å^{-1}$, and the total energy change is below 10^{-5} eV [40].

3. Results and Discussion

3.1. Structure and Adsorption Characteristics

For intrinsic g−ZnO, the lattice constant, the Zn-O bond length, and the bond angle of Zn-O-Zn are a = 3.289 Å, 1.899 Å, and 120°, respectively. These results aligned with the previously reported [41]. To obtain the most stable adsorption conformation, four adsorption sites were considered, as shown in Figure 1a. To research the intrinsic g−ZnO adsorption system, the DOS of the intrinsic g−ZnO was calculated and displayed in Figure 1b. The DOS shows that spin up and down components of the intrinsic g−ZnO are symmetric, indicating that the intrinsic g−ZnO is non-magnetic. Moreover, the valence band maxima of intrinsic g−ZnO are mainly determined by the O atom, while the conduction band minima are determined primarily by the Zn atom.

For the defective g−ZnO, two defect types (Zinc vacancy and Oxygen vacancy) were considered, as depicted in Figure 1c,e, respectively. For the Zinc vacancy g−ZnO (V_{Zn}/g−ZnO), O atoms around the V_{Zn} are all far away from the vacancy canter. Moreover, the Zn-O bond length around the V_{Zn} decreases to 1.832 Å, and the bond angle of Zn-O-Zn increases to 134.093°. The reason for this phenomenon is that the charge of the adjacent atom is transferred to the vacancy after the Zn atom is removed, and the V_{Zn} becomes a negative electric center, which has a positive Coulomb repulsion potential [42]. Huang et al. [43] calculated that the change of Zn-O-Zn bond angle around the vacancy of V_{Zn}/g−ZnO increases to 133.79°, and our results are similar. However, for the Oxygen vacancy g−ZnO (V_O/g−ZnO), the three Zn atoms around the V_O are all near the vacancy center. The O-Zn bond length around V_O increases to 1.946 Å, and the bond angle of O-Zn-O decreases to 107.336°, consistent with previous reports [43,44]. The reason is that the charge density around the vacancy changes after the Zn atom is removed, and the V_O becomes a positive electric center with a negative Coulomb attraction potential [45].

To probe into the gas adsorbed on the defective g−ZnO system, the DOS of V_{Zn}/g−ZnO was calculated and displayed in Figure 1d. It can be observed that the spin up and down is asymmetric. The spin-down impurity levels appear at 0.099 eV and 0.311 eV above the Fermi level, indicating that the introduction of V_{Zn} induces the production of magnetic. The V_{Zn}/g−ZnO have magnetic moment of 1.996 μ_B. In addition, the DOS shows that the impurity levels are mainly devoted by the O atom. The DOS of V_O/g−ZnO were calculated and displayed in Figure 1f. It can be observed that no magnetic properties are generated after the introduction of V_O. The DOS indicates that valence band maxima is mainly contributed by the O atoms, and conduction band minima is mainly by the Zn atoms.

The most stable structure of gas (CO, NH_3, NO, and NO_2) adsorbed on intrinsic g−ZnO system is shown in Figure 2a–e. Overall, CO, NH_3, and NO molecules are tilted concerning the intrinsic g−ZnO plane, and the C-atom, N-atom, and N-atom near the intrinsic g−ZnO aircraft, respectively. In contrast, the NO_2 molecule, with the O atom close to the intrinsic g−ZnO aircraft, is parallel to the intrinsic g−ZnO plane. In addition, the adsorption sites for CO, NH_3, NO, and NO_2 molecules are A_C, A_C, A_{Zn}, and A_O, respectively. The most stable configurations of gas adsorbed on the V_{Zn}/g−ZnO system and the V_O/g−ZnO system are shown in Figure 2f–h and 2i–l, respectively. For the gas adsorbed on V_{Zn}/g−ZnO systems, gas molecules are tilted to V_{Zn}/g−ZnO, and nearly embedded in V_{Zn}/g−ZnO. For CO molecules, the C atom is closer to the V_{Zn}/g−ZnO, while the H atom is for NH_3 molecules. For NO and NO_2 molecules, the N atom is closer to the V_{Zn}/g−ZnO plane. For the gas adsorbed on V_O/g−ZnO systems, all gas molecules are inclined to V_O/g−ZnO. The difference is that the N atoms of the NH_3 is closer to the V_O/g−ZnO. And, for the NO_2 molecule, the O atom is closer to the V_O/g−ZnO plane.

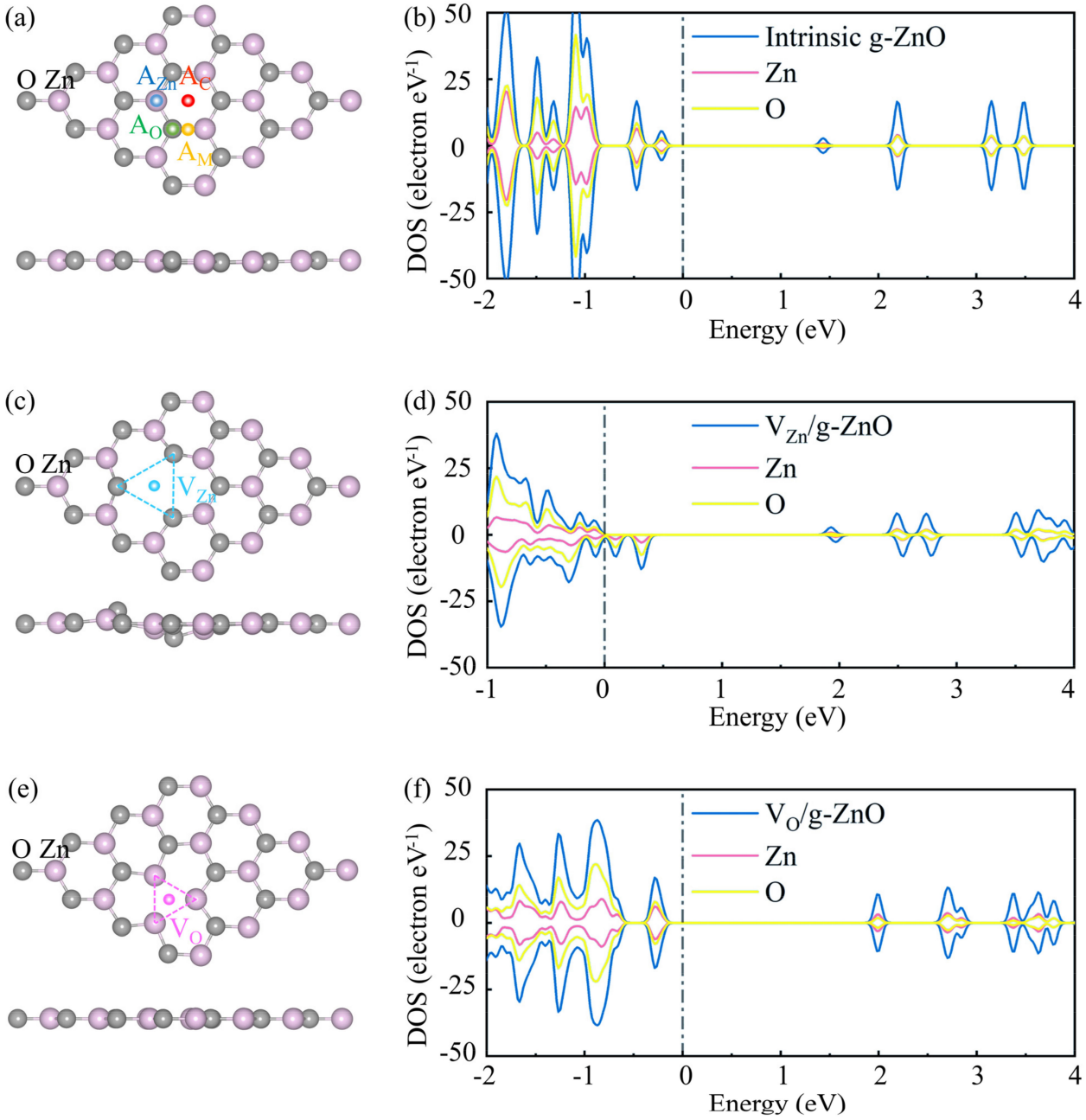

Figure 1. (**a**) The crystal structure and (**b**) DOS of intrinsic g−ZnO. A_{Zn} is above the Zn atom. (**c**) The crystal structure and (**d**) the DOS of Zinc vacancy g−ZnO (V_{Zn}/g−ZnO), and (**e**) The crystal structure and (**f**) the DOS of Oxygen vacancy g−ZnO (V_O/g−ZnO). A_O is upper the O atom, A_M is upper the bond of Zn-O, and A_C is upper the center of the hexagonal structure. V_{Zn} is upper the Zn vacancy, and V_O is above the O vacancy. The pink spheres represent Zn atoms, and the grey spheres represent O atoms. The Fermi level is shifted to 0 eV.

To explore the sensitivity of the subject material to gas molecules and the type of adsorption, the E_{ad} and adsorption height was shown in Figures 3 and 4, respectively. Overall, the E_{ad} are all negative, indicating that the adsorption process of each system is exothermic and stable. Moreover, the absolute values of adsorption energy of V_{Zn}/g−ZnO adsorbed by CO, NH_3, NO, and NO_2 systems are higher than other adsorption systems. It shows that V_{Zn}/g−ZnO is suitable for detecting four gas molecules [46]. In addition, the intrinsic g−ZnO showed the best detection capability for NH_3 gas molecules. In comparison, due to the introduction of defects, the V_{Zn}/g−ZnO adsorption systems showed the

most significant improvement in detecting NO and NO_2 gas. And V_O/g−ZnO adsorption systems showed the most remarkable enhancement in detecting NO_2 gas molecules.

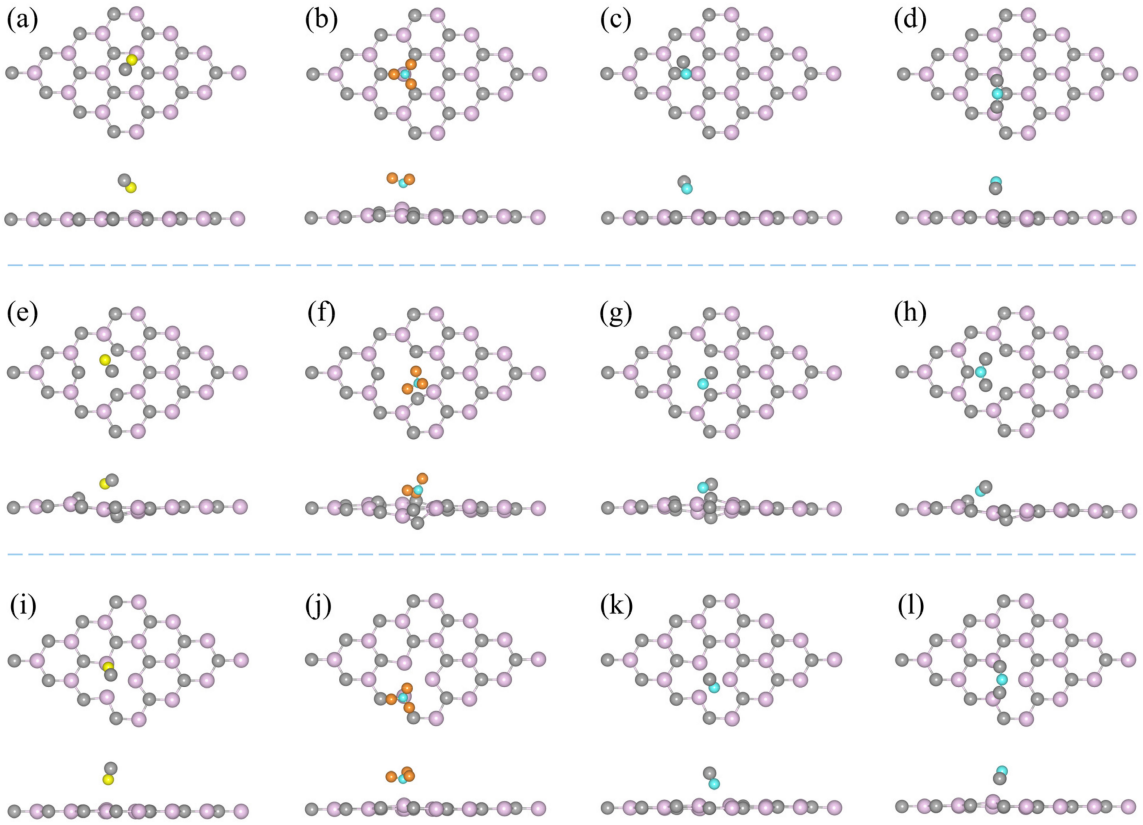

Figure 2. The stable structures of (**a**) CO, (**b**) NH_3, (**c**) NO, or (**d**) NO_2 adsorbed on intrinsic g−ZnO systems, (**e**–**h**) V_{Zn}/g−ZnO systems, and (**i**–**l**) V_O/g−ZnO systems. The pink, grey, yellow, orange, and blue balls represent Zn, O, C, H, and N atoms, respectively.

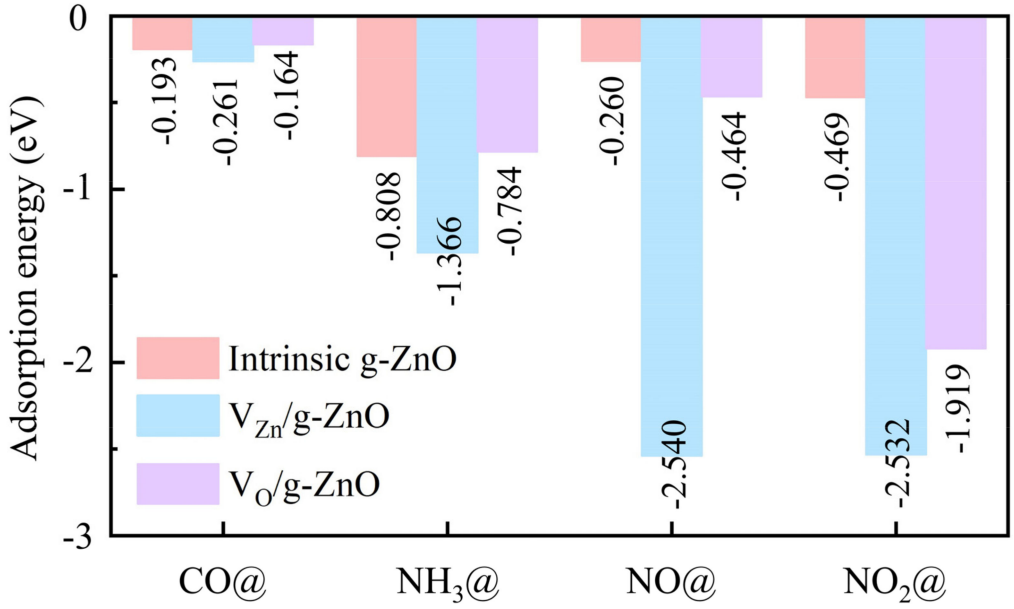

Figure 3. The absorption energy of gas molecules on intrinsic g−ZnO, V_{Zn}/g−ZnO, and V_O/g−ZnO systems.

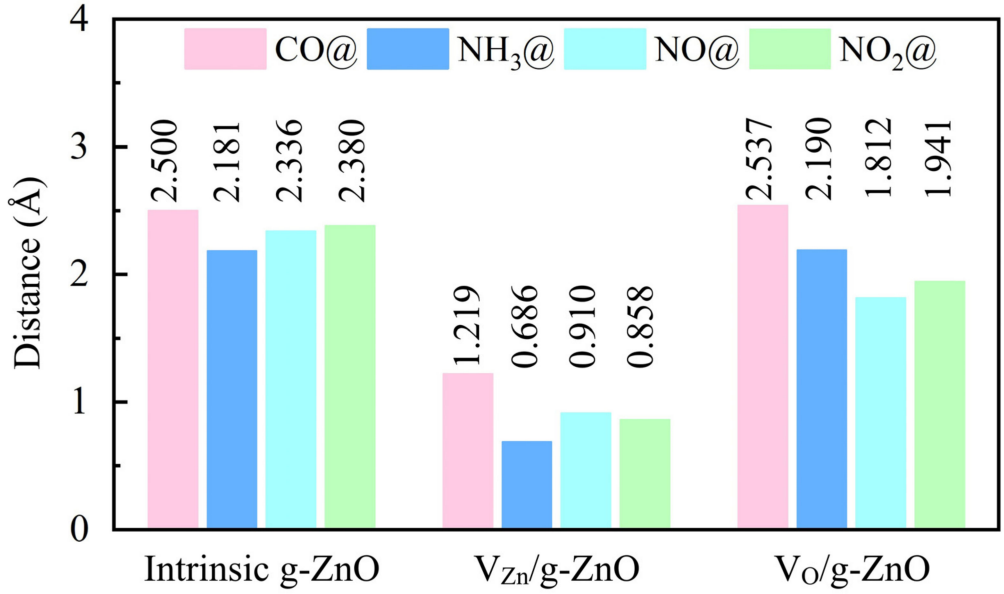

Figure 4. The absorption height of gas molecules on intrinsic g−ZnO, V_{Zn}/g−ZnO, and V_O/g−ZnO systems.

The calculated adsorption height is defined as the closest atomic spacing between the gas and the g−ZnO or defective g−ZnO [5,47]. For the gas adsorbed on intrinsic g−ZnO system, the adsorption heights of the intrinsic g−ZnO adsorbed by CO gas (CO@ g−ZnO) system are 2.500 Å, more significant than the Zn-C bond length (2.010 Å [48]). The adsorption heights of the adsorption of intrinsic g−ZnO by NO gas (NO@ g−ZnO) system are 2.336 Å, larger than the Zn-O (1.950 Å [49]) or O-O (1.410 Å [50]) bond length. The adsorption heights of the adsorption of intrinsic g−ZnO by NO_2 gas (NO_2@ g−ZnO) system are 2.380 Å, bigger than the Zn-O bond length. The smaller E_{ad} and larger adsorption height indicate that these are physical adsorption. On the contrary, the adsorption heights of the NH_3 gas adsorbed on the intrinsic g−ZnO (NH_3@ g−ZnO) system are 2.181 Å, which is less than the Zn-N bond length (2.22~2.25 Å [51,52]), and its larger E_{ad} proves to be chemisorption. For the gas adsorption V_{Zn}/g−ZnO systems, the adsorption heights of the V_{Zn}/g−ZnO systems for CO, NH_3, NO, and NO_2 adsorption are 1.219 Å, 0.686 Å, 0.910 Å, and 0.858 Å, respectively. The adsorption height of the V_{Zn}/g−ZnO adsorbed by CO (CO@ V_{Zn}/g−ZnO) system is greater than the O-C bond length (1.136 Å [53]), and its smaller adsorption energy demonstrates physical adsorption. The NH_3 adsorbed on V_{Zn}/g−ZnO (NH_3@ V_{Zn}/g−ZnO) system, the NO adsorbed on V_{Zn}/g−ZnO (NO@ V_{Zn}/g−ZnO) system, and NO_2 adsorbed on V_{Zn}/g−ZnO (NO_2@ V_{Zn}/g−ZnO) system have smaller adsorption heights and larger adsorption energy indicating that they are chemisorbed. The smaller adsorption height, the stronger the interaction between layers [46]. For the gas adsorption V_O/g−ZnO systems, the adsorption height of the V_O/g−ZnO adsorbed by CO (CO@ V_O/g−ZnO) system is 2.537 Å, which is higher than the Zn-C bond length and have smaller adsorption energy. Thus, it is physical adsorption. For the NH_3 adsorbed on V_O/g−ZnO (NH_3@ V_O/g−ZnO) system, NO adsorbed on V_O/g−ZnO (NO@ V_O/g−ZnO) system, and NO_2 adsorbed on V_O/g−ZnO (NO_2@ V_O/g−ZnO) system, the adsorption heights are 2.190 Å, 1.812 Å, and 1.941 Å, respectively, which are less than the Zn-N, Zn-N, and Zn-O bond lengths, respectively, and are chemisorption.

3.2. Electronic Characteristics

To explore the interaction mechanism of the adsorption process between the gas molecules and the host material, the CDD was calculated for each system. Figure 5a–d illustrates the CDD of the intrinsic g−ZnO adsorption systems. For the CO@ g−ZnO system, the electrons lost by the C atom in the CO gas and the Zn atom below are mainly

captured by the CO molecule and the O atom in g−ZnO. However, for the NH_3@ g−ZnO system, the electron is mainly distributed between the NH_3 molecule and the g−ZnO layer, which may be used to form chemosynthetic bonds consistent with the chemisorption in the previous section. For the NO@ g−ZnO system, the electrons lost by the Zn atoms below the NO molecule are mainly distributed around the NO molecule. For NO_2@ g−ZnO system, it is similar to the NO system, but the difference is that NO_2 molecules capture more electrons. To obtain precise charge transfer amounts, Bader charges were calculated as listed in Table 1a. What can be found is that CO, NO, and NO_2 molecules act as electron acceptors, receiving 0.007e, 0.083e, and 0.252e from the intrinsic g−ZnO, respectively. Since the polarity of NO_2 molecules is higher than that of CO and NO molecules, the charge transfer of the NO_2@ g−ZnO system is significantly higher than that of the CO@ g−ZnO and NO@ g−ZnO systems. However, NH_3 molecules act as electron donors with 0.111e charge transfer to the intrinsic g−ZnO.

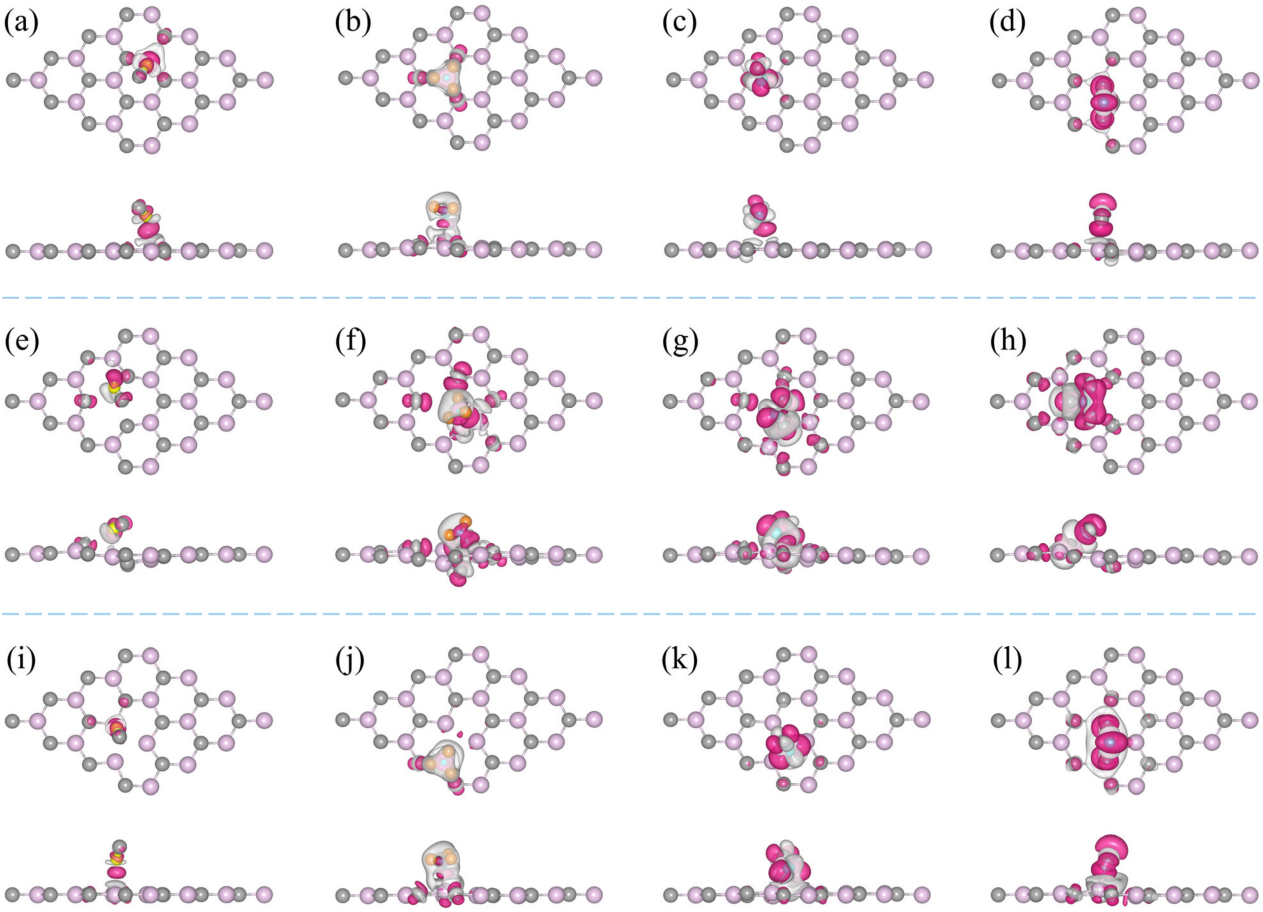

Figure 5. The isosurface of the CDD with a value of 0.001 e $Å^{-3}$ for the (**a**) CO, (**b**) NH_3, (**c**) NO, or (**d**) NO_2 adsorbed on intrinsic g−ZnO systems, (**e**–**h**) for the V_{Zn}/g−ZnO adsorption systems, and (**i**–**l**) for the V_O/g−ZnO adsorption systems. The white area and peachy red area represent the depletion and accumulation of electrons, respectively. The pink, grey, yellow, orange, and blue balls are the Zn, O, C, H, and N atoms, respectively.

Table 1. The magnetic moments (M_{total}), bandgap (E_g), and charge transfer (ΔQ) for the stable configurations of gas adsorbed on intrinsic g−ZnO, V_{Zn}/g−ZnO, and V_O/g−ZnO.

Adsorption System Type	Configuration	M_{total} (μ_B)	E_g (eV)	ΔQ (e)
Intrinsic	CO	0	1.683	0.007
	NH_3	0	1.645	−0.111
	NO	1	1.717	0.083
	NO_2	0.858	0	0.252
Zn-vacancy	CO	1.967	0.089	0.019
	NH_3	1.191	0	−0.110
	NO	1	1.882	−0.110
	NO_2	1	1.828	0.017
O-vacancy	CO	0	2.140	0.012
	NH_3	0	2.151	−0.101
	NO	1	0.808	0.312
	NO_2	1	0.233	0.626

The CDD notations for the gas molecule adsorption V_{Zn}/g−ZnO systems and the gas molecule adsorption V_O/g−ZnO systems are shown in Figures 5e–h and 5i–l, respectively. The Bader charge calculation is displayed in Table 1b,c, respectively. For the CO adsorption defective g−ZnO system, the charge transfers amounts for the CO@ V_{Zn}/g−ZnO system and CO@ V_O/g−ZnO system are 0.019e and 0.017e, respectively, and both are transferred from the defective g−ZnO to the CO gas. Compared with the CO@ g−ZnO system, the charge transfer amounts are increased, and the corresponding regions of CO-gaining electrons are larger. For the NH_3 adsorbed defective g−ZnO systems, NH_3 still acts as an electron donor, transferring 0.110e and 0.101e to the V_{Zn}/g−ZnO and V_O/g−ZnO layers, respectively, with no significant change in charge transfer compared to the CO@ g−ZnO system. However, for the NO adsorption defective g−ZnO system, in the NO@ V_{Zn}/g−ZnO system, NO was converted from an electron acceptor to an electron donor and provided 0.110e to the V_{Zn}/g−ZnO layer. In the NO@ V_O/g−ZnO system, NO receives 0.312e from the V_O/g−ZnO layer as an electron acceptor, and the charge transfer is significantly increased compared to the NO@ g−ZnO system. And the charge density around NO is also increased considerably. In the NO_2@ V_{Zn}/g−ZnO system. 0.017e is transferred from the V_{Zn}/g−ZnO to the NO_2 gas. The charge density around NO_2 decreased substantially compared to the NO_2@ g−ZnO system. In contrast, in the NO_2@ V_O/g−ZnO system, NO_2 acts as an electron acceptor and receives 0.626e from the V_O/g−ZnO layer, and the amount of charge transfer and the charge density around NO_2 increases dramatically.

The band structure was calculated to research the effect of defects further. The band structure of the intrinsic g−ZnO is shown in Figure 6a for comparative study. The intrinsic g−ZnO has a direct bandgap (1.651 eV) at the Γ point. Hu et al. [54] used a similar algorithm to calculate the bandgap of the intrinsic g−ZnO is 1.670 eV, which is consistent. The band structure of the intrinsic g−ZnO adsorption systems is displayed in Figure 6b–e. It can be observed that the band structure of the CO@ g−ZnO system and NH_3@ g−ZnO system have not significantly changed compared to that of the intrinsic g−ZnO, remaining non-magnetic direct bandgap with the value of 1.683 eV and 1.645 eV, respectively. Similar results were obtained by Zhou et al. [55] in a study of WS_2 adsorption by CO and NH_3 gases. For the NO@ g−ZnO system and NO_2@ g−ZnO system, a splitting of the spin up and down bands can be noted, indicating that the adsorption of NO and NO_2 induces magnetic properties. For the NO@ g−ZnO system, NO turns into a magnetic direct bandgap semiconductor with a value of 1.717 eV, while the CBM of the NO_2@ g−ZnO system crosses the Fermi level and exhibits metallic behavior. Besides, in the NO@ g−ZnO system, spin-up impurity energy bands appear near −0.237 eV and 0.320 eV on both sides of the Fermi energy level and spin-down impurity energy bands appear at 0.676 eV above the Fermi energy level, presumably introduced by NO. Moreover, in the NO_2@ g−ZnO system, a spin-down impurity energy level appears near the Fermi energy level, which may be

provided by NO_2. Similarly, in NO and NO_2 adsorption of transition metal-doped MoS_2 has been reported by Salih et al. [56]. A similar statement was made in the study of gas adsorption of WS_2 by Zhou et al. [55]

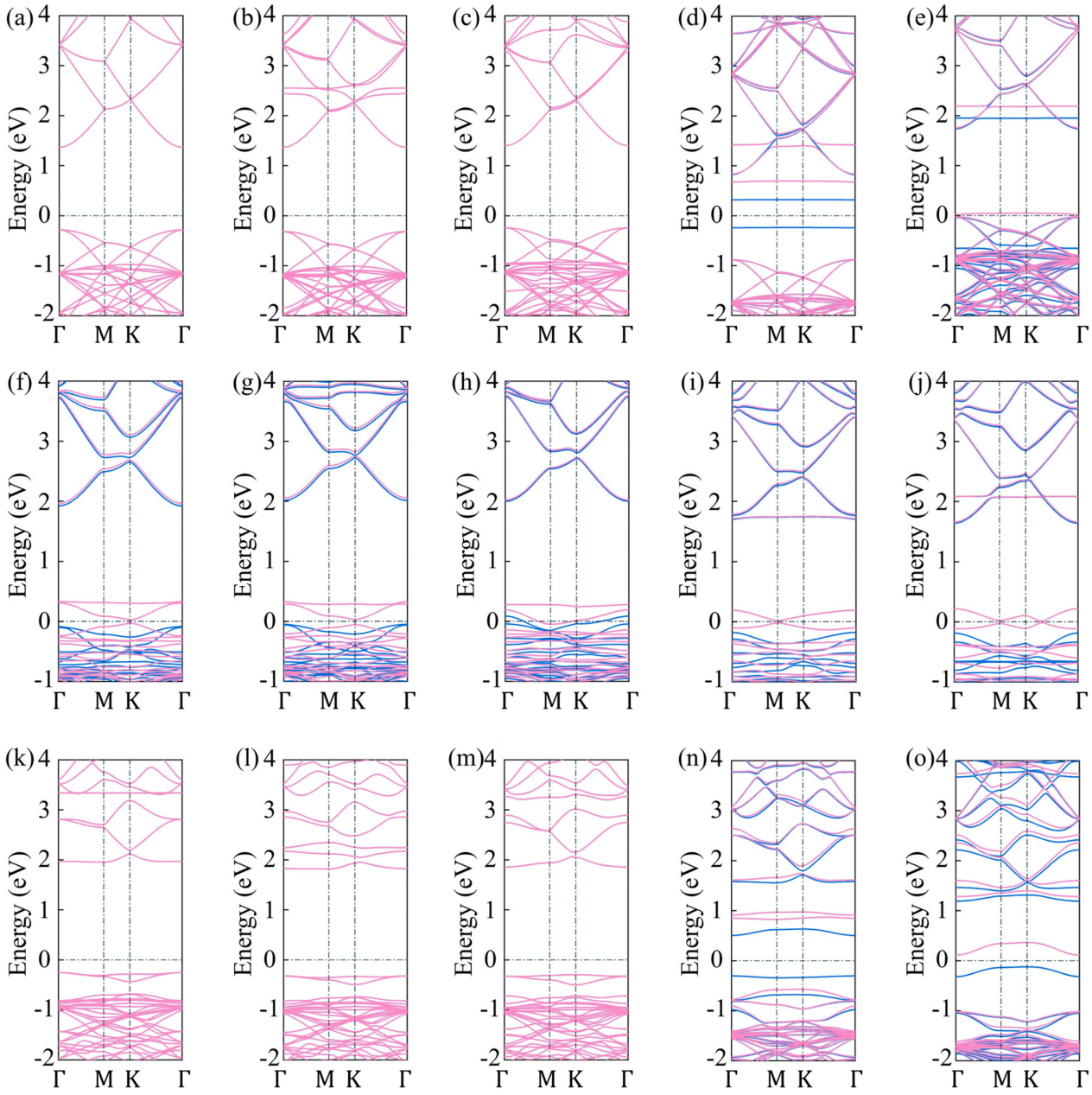

Figure 6. The band structures of (**a**) intrinsic g−ZnO, and (**b**) CO, (**c**) NH_3, (**d**) NO, or (**e**) NO_2 adsorbed on intrinsic g−ZnO systems. The band structures of (**f**) V_{Zn}/g−ZnO, and (**g**) CO, (**h**) NH_3, (**i**) NO, or (**j**) NO_2 adsorbed on V_{Zn}/g−ZnO systems. The band structures of (**k**) V_O/g−ZnO, and (**l**) CO, (**m**) NH_3, (**n**) NO, or (**o**) NO_2 adsorbed on V_O/g−ZnO systems. The dark blue and pink lines denote spin up and down, respectively. The Fermi level is set to 0 eV.

The band structure of V_{Zn}/g−ZnO is displayed in Figure 6f as a comparison and exhibits magnetic semiconductor properties at K with a direct bandgap of 0.058 eV. The band structure of the V_{Zn}/g−ZnO adsorption system is shown in Figure 6g–j. It can be observed that for the CO@ V_{Zn}/g−ZnO system, there is no significant change compared to that of V_{Zn}/g−ZnO, which is still a magnetic direct bandgap semiconductor at K, and the value is 0.089 eV. However, for the NH_3@ V_{Zn}/g−ZnO system, the band structure shows

spin up and down bands crossing the Fermi level, indicating that the NH_3@ V_{Zn}/g−ZnO system exhibits magnetic metallic behavior. For the NO@ V_{Zn}/g−ZnO system and NO_2@ V_{Zn}/g−ZnO system, the band structures exhibit semi-metallic properties, with the spin-down band structure crossing the Fermi energy level to exhibit metallic behavior. In contrast, the spin-up band structure maintains the semiconductor properties. The spin-up bandgap values are 1.882 eV and 1.828 eV, respectively.

The band structure of V_O/g−ZnO is displayed in Figure 6k as a comparison, and shows that V_O/g−ZnO have a non-magnetic direct bandgap (2.208 eV) at Γ. The band structure of the V_O/g−ZnO adsorption system is shown in Figure 6l–o. From the figure, it can be understood that the CO and NH_3 molecules have little effect on V_O/g−ZnO. These show that the non-magnetic direct semiconductor properties are still maintained, with values of 2.140 eV and 2.151eV, respectively in the CO@ V_O/g−ZnO system and NH_3@ V_O/g−ZnO system. However, for the NO@ V_O/g−ZnO system and NO_2@ V_O/g−ZnO system, the band structure shows spin up and down splitting, indicating the appearance of magnetic behavior. Due to the adsorption of NO and NO_2, the V_O/g−ZnO transforms into a magnetic semiconductor. The bandgap of the NO@ V_O/g−ZnO system and the NO_2@ V_O/g−ZnO system are 0.808 eV and 0.233 eV, respectively.

3.3. Magnetism

To reveal the band structure composition and the origin of the magnetism, the DOS and the spin density are researched. The DOS of gas adsorbed on intrinsic g−ZnO are displayed in Figure 7. What can be observed is that the states contributed by CO and NH_3 gas molecules have less effect on the intrinsic g−ZnO. However, NO and NO_2 gas molecules have a more significant impact on the DOS of intrinsic g−ZnO. The DOS of the NO@ g−ZnO system shows that the DOS is asymmetric in the upper and lower Brillouin zone. The spin-up impurity levels on both sides of the Fermi level, and those above the Fermi level are mainly contributed by NO gas. It indicates that the adsorption of NO introduces magnetic properties.

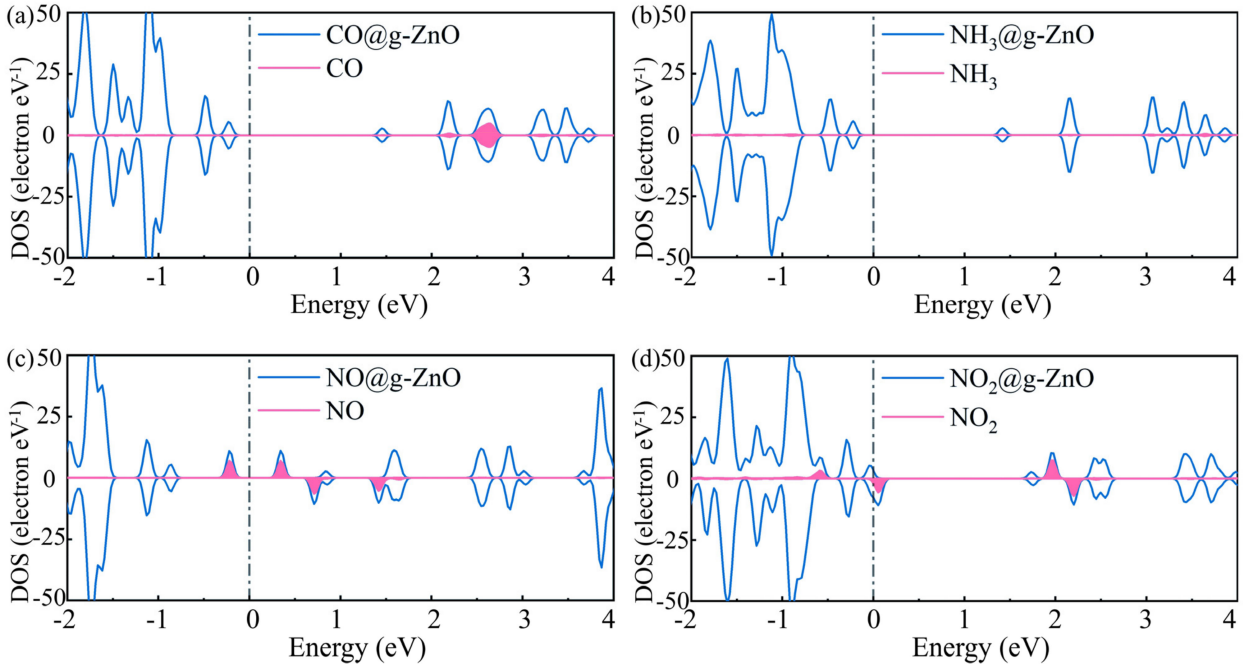

Figure 7. The DOS of (**a**) CO, (**b**) NH_3, (**c**) NO, or (**d**) NO_2 adsorbed on intrinsic g−ZnO systems. The Fermi level is shifted to 0 eV and respected by a black dash line.

The spin density, as shown in Figure 8a, confirms that the magnetic moment is mainly from NO gas molecules, and the magnetic moment is 1 μ_B. The Brillouin zone above and

below the DOS of the NO_2@ g−ZnO system is also asymmetric. The spin-down impurity level near the Fermi level is mainly contributed by NO_2, and it crosses the Fermi level. And the spin-up is also. This suggests that the adsorption of NO_2 not only introduces magnetic properties but makes the NO_2@ g−ZnO system exhibit metal properties. The spin density shown in Figure 8b shows that the magnetic of the NO_2@ g−ZnO system comes from the NO_2 gas molecule, but a small part of the magnetic moment comes from the O atom below the NO_2 gas. The magnetic moment is 0.858 μ_B. Consistent with the band structure results.

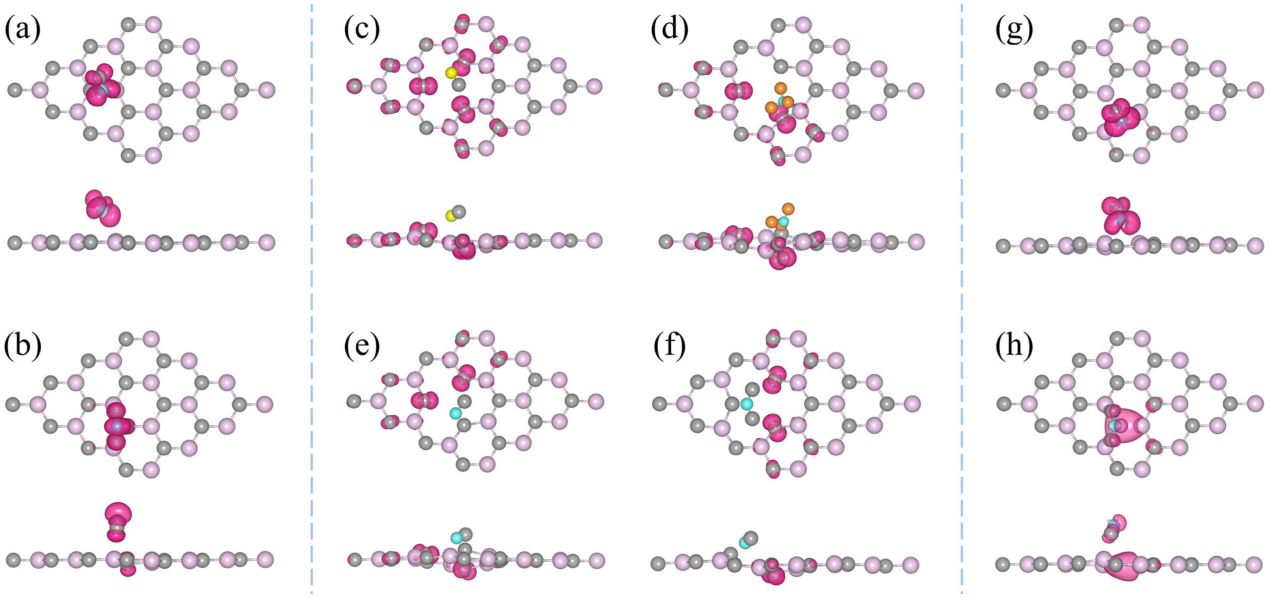

Figure 8. The spin density of (**a**) NO, or (**b**) NO_2 molecules adsorbed on intrinsic g−ZnO, of (**g**,**h**) V_O/g−ZnO adsorption systems, and of (**c**) CO, (**d**) NH_3, (**e**) NO, or (**f**) NO_2 molecules adsorbed on V_{Zn}/g−ZnO systems. The peachy red area denotes the spin-up, whereas the white area represents the spin-down. The pink, grey, yellow, orange, and blue balls are the Zn, O, C, H, and N atoms, respectively.

The DOS of the V_{Zn} and V_O g−ZnO adsorption systems are shown in Figures 9 and 10, respectively. What can be observed is that the DOS of the upper and lower Brillouin zone of the V_{Zn}/g−ZnO adsorption systems are asymmetric due to the magnetic properties of V_{Zn}/g−ZnO, indicating that all adsorption systems possess magnetic properties. Besides, it can be found that CO gas molecules do not contribute to the forbidden band of V_{Zn}/g−ZnO, and the CO@ V_{Zn}/g−ZnO system is still a narrow bandgap magnetic semiconductor. Although the NH_3 gas molecules hardly contribute to the total DOS, the NH_3 causes the spin up and down DOS to cross the Fermi level, making the NH_3@ V_{Zn}/g−ZnO system exhibit metallic behavior. In the NO@ V_{Zn}/g−ZnO system, NO makes the spin-down DOS cross the Fermi level, making it exhibit semi-metallic properties. The NO_2@ V_{Zn}/g−ZnO system is similar to the NO@ V_{Zn}/g−ZnO system, except that the NO_2 gas molecules do not induce the production of impurity energy levels in the V_{Zn}/g−ZnO forbidden band. Not surprisingly, the magnetic of the CO@, NH_3@, NO@, and NO_2@ V_{Zn}/g−ZnO systems are mainly contributed by the uncoordinated O atoms around V_{Zn}, and the gas molecules do not contribute to the magnetic moments in Figure 8c–f. The magnitudes of the magnetic moments are 1.967 μ_B, 1.191 μ_B, 1 μ_B, and 1 μ_B.

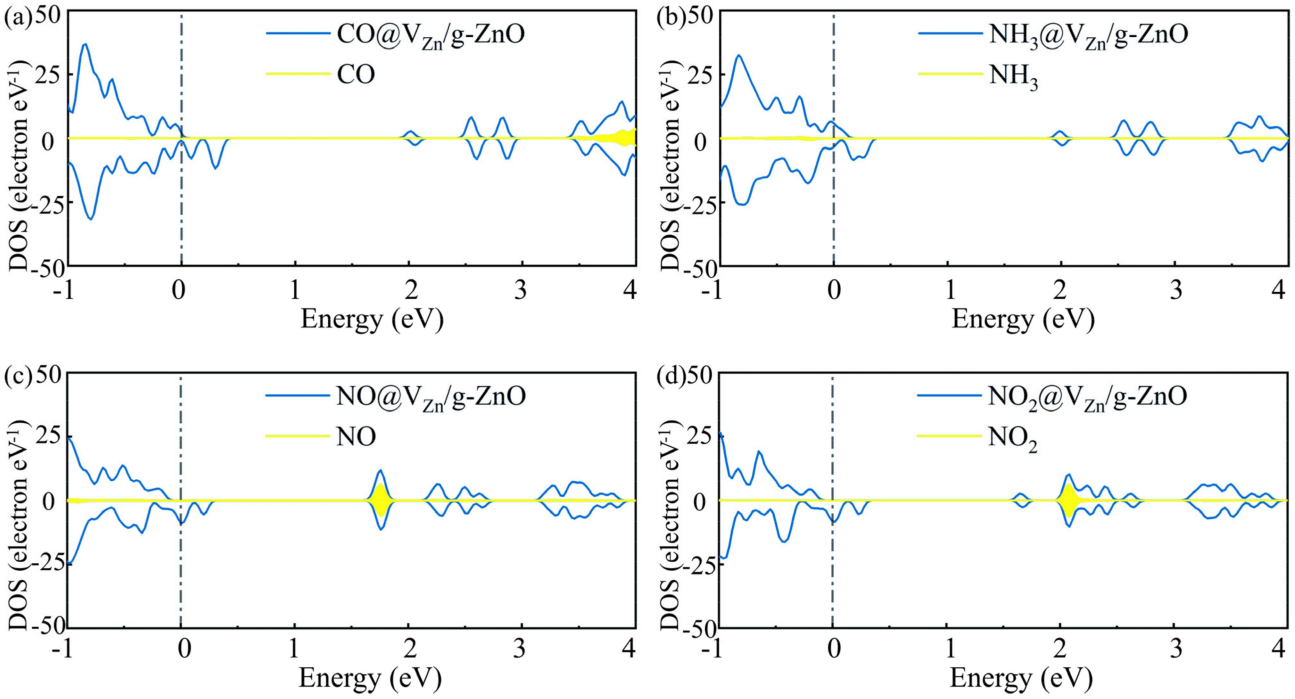

Figure 9. DOS of (**a**) CO, (**b**) NH_3, (**c**) NO, or (**d**) NO_2 adsorbed on $V_{Zn}/g-ZnO$ systems.

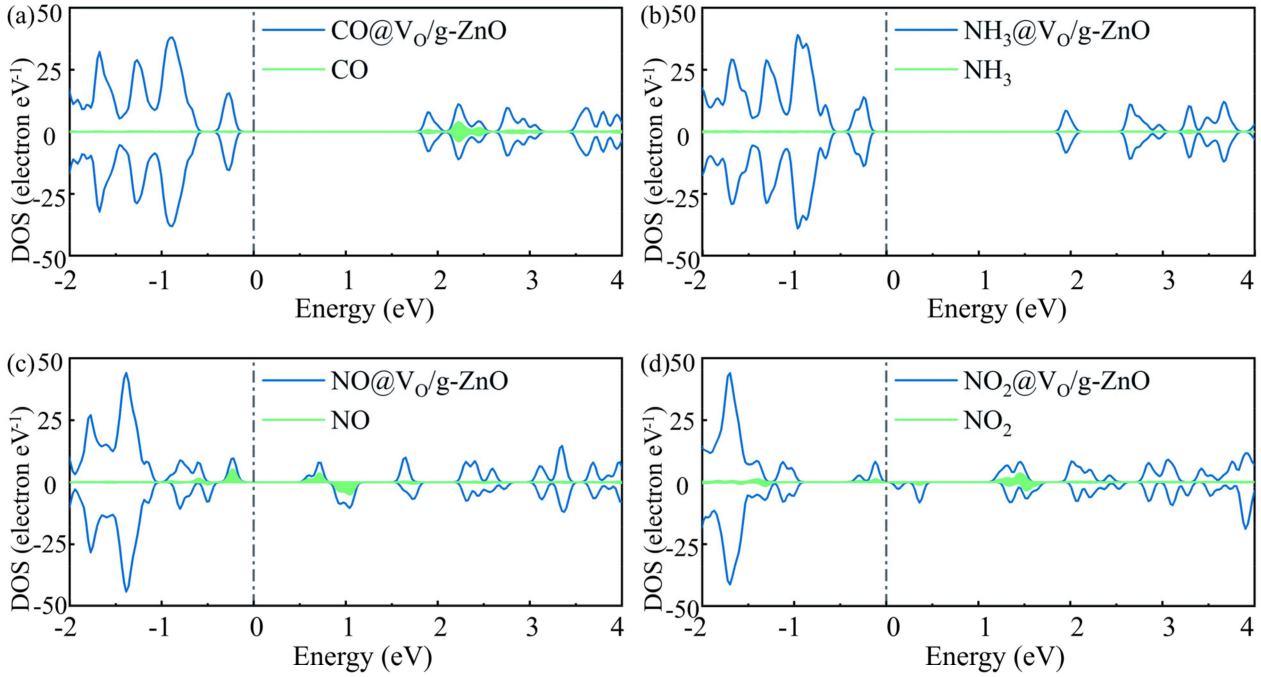

Figure 10. DOS of (**a**) CO, (**b**) NH_3, (**c**) NO, or (**d**) NO_2 adsorbed on $V_O/g-ZnO$ systems.

For the gas adsorption $V_O/g-ZnO$ system, the CO and NH_3 gas molecules have no contribution within the forbidden band of $V_O/g-ZnO$, and the NH_3 gas molecules have almost no contribution to the total DOS. Therefore, no significant change in DOS compared to that of $V_O/g-ZnO$. The DOS of the NO@ $V_O/g-ZnO$ system and the NO_2@ $V_O/g-ZnO$ system are asymmetric in the upper and lower Brillouin zone, suggesting that the adsorption of NO and NO_2 gases induces magnetism. In the NO@ $V_O/g-ZnO$ system, the VBM and CBM are mainly contributed by NO gas molecules. However, in the NO_2@ $V_O/g-ZnO$ system, the NO_2 contribution to the in-band DOS of $V_O/g-ZnO$ is not

apparent. Correspondingly, the magnetic moments of the NO@ V_O/g−ZnO system, as shown in Figure 8g, mainly originate from NO gas molecules, while the magnetic moments of the NO_2@ V_O/g−ZnO system mainly come from the Zn atoms near V_O as displayed in Figure 8h. The magnetic moments of the NO@ V_O/g−ZnO system and NO_2@ V_O/g−ZnO system are 1 μ_B and 1 μ_B, respectively.

4. Conclusions

In summary, the adsorption of CO, NH_3, NO, and NO_2 gas molecules on intrinsic g−ZnO and vacancy g−ZnO were systematically studied by the first principle based on DFT. the E_{ad}, adsorption height, CDD, band structure, DOS, and spin density of the magnetic systems for each adsorption system were considered. The effect of vacancies on the interaction between g−ZnO and gas, and on the electronic properties were investigated. In addition, the source of magnetic generation is revealed. The results show that the adsorption energy is promoted, and the adsorption height is reduced due to the introduction of defects. Compared with the NH_3@, NO@, and NO_2@ g−ZnO systems, the E_{ad} of the NH_3@, NO@, and NO_2@ V_{Zn}/g−ZnO systems increased to 1.366 eV, 2.540 eV, and 2.532 eV, respectively. The adsorption height was significantly reduced to 0.686 Å for the NH_3@ V_{Zn}/g−ZnO system. It is worth mentioning that the NH_3, NO, and NO_2 gas molecules adsorbed on the defective g−ZnO system are converted to chemical adsorption due to the larger adsorption energy and smaller adsorption height. The CDD indicate that the introduction of V_O significantly enhances the charge transfer between NO and NO_2 and V_O/g−ZnO. The band structure, DOS, and spin density results show that the introduction of V_{Zn} splits the spin-up band and spin-down band structures, producing a magnetic moment value of 1.996 μ_B for g−ZnO. NO and NO_2 gases can induce the magnetic properties of intrinsic g−ZnO (1 μ_B and 0.858 μ_B) and V_O/g−ZnO (1 μ_B and 1 μ_B), while the adsorption of gases can degrade the magnetic properties of V_{Zn}/g−ZnO itself (1.967 μ_B, 1.191 μ_B, 1 μ_B, and 1 μ_B). Notably, the adsorption of NO_2 causes the intrinsic g−ZnO to show metallic properties, while the adsorption of NH_3 gas molecules causes V_{Zn}/g−ZnO to also exhibit metallic properties. The adsorption of NO and NO_2 causes V_{Zn}/g−ZnO to exhibit semi-metallic properties. These are beneficial to enrich the detection means of defects and the design of gas detection devices [57].

Author Contributions: Conceptualization, Y.S., Z.C. and E.L.; methodology, D.M.; software, Z.C.; validation, Y.S., Z.C., D.M., P.Y., K.Y., Y.D., F.W. and E.L.; formal analysis, Z.Y.; investigation, Z.Y., P.Y., K.Y., Y.D. and F.W.; resources, Z.C. and E.L.; data curation, Z.Y.; writing—original draft preparation, Y.S. and Z.Y.; writing—review and editing, Y.S.; visualization, Z.Y.; supervision, Y.S., Z.C. and E.L.; project administration, E.L.; funding acquisition, Y.S. and Z.C. All authors have read and agreed to the published version of the manuscript.

Funding: This work was funded by the Natural Science Basic Research Program of Shaanxi (Program No. 2022JM-176), Scientific Research Program Funded by Shaanxi Provincial Education Department (Program No. 21JK0789), Xi'an Science and Technology Project (Program No. 22GXFW0080), the Opening Project of Shanghai Key Laboratory of Special Artificial Microstructure Materials and Technology (Program No. ammt2020A-6), College Students' Innovative Entrepreneurial Training Plan Program (Program No. 202210700008 and Program No. 202210700105), the National Natural Science Foundation of China (No. 12104362) and China Postdoctoral Science Foundation (Program No. 2020M683684XB).

Institutional Review Board Statement: Not applicable.

Informed Consent Statement: Not applicable.

Data Availability Statement: The raw data supporting the conclusions of this article will be made available by the authors, without undue reservation.

Conflicts of Interest: The authors declare no conflict of interest.

References

1. Barik, S.; Srivastava, A.; Misra, P.; Nandedkar, R.; Kukreja, L. Alumina capped ZnO quantum dots multilayer grown by pulsed laser deposition. *Solid State Commun.* **2003**, *127*, 463–467. [CrossRef]
2. Wang, Z.L. Nanostructures of zinc oxide. *Mater. Today* **2004**, *7*, 26–33. [CrossRef]
3. Fouad, O.; Ismail, A.; Zaki, Z.; Mohamed, R. Zinc oxide thin films prepared by thermal evaporation deposition and its photocatalytic activity. *Appl. Catal. B Environ.* **2006**, *62*, 144–149. [CrossRef]
4. Cui, Z.; Wang, X.; Li, M.; Zheng, J.; Ding, Y.; Liu, T. Tuning the optoelectronic properties of graphene-like GaN via adsorption for enhanced optoelectronic applications. *Solid State Commun.* **2019**, *296*, 26–31. [CrossRef]
5. Meng, R.; Lu, X.; Ingebrandt, S.; Chen, X. Adsorption of Gas Molecules on Graphene-Like ZnO Nanosheets: The Roles of Gas Concentration, Layer Number, and Heterolayer. *Adv. Mater. Interface* **2017**, *4*, 1700647. [CrossRef]
6. Shen, Y.; Yuan, Z.; Cui, Z.; Ma, D.; Yang, K.; Dong, Y.; Wang, F.; Du, A.; Li, E. Electronic, Magnetic, and Optical Properties of Metal Adsorbed g−ZnO Systems. *Front. Chem.* **2022**, *10*, 943902. [CrossRef]
7. Long, H.; Fang, G.; Li, S.; Mo, X.; Wang, H.; Huang, H.; Jiang, Q.; Wang, J.; Zhao, X. A ZnO/ZnMgO multiple-quantum-well ultraviolet random laser diode. *IEEE Electron. Device Lett.* **2010**, *32*, 54–56. [CrossRef]
8. Tusche, C.; Meyerheim, H.; Kirschner, J. Observation of depolarized ZnO (0001) monolayers: Formation of unreconstructed planar sheets. *Phys. Rev. Lett.* **2007**, *99*, 026102. [CrossRef]
9. Cui, Z.; Ren, K.; Zhao, Y.; Wang, X.; Shu, H.; Yu, J.; Tang, W.; Sun, M. Electronic and optical properties of van der Waals heterostructures of g-GaN and transition metal dichalcogenides. *Appl. Surf. Sci.* **2019**, *492*, 513–519. [CrossRef]
10. Liu, J.; Gao, F.; Wu, L.; Zhang, H.; Hong, W.; Jin, G.; Zhai, Z.; Fu, C. Size effect on oxygen vacancy formation and gaseous adsorption in ZnO nanocrystallites for gas sensors: A first principle calculation study. *Appl. Phys. A* **2020**, *126*, 454. [CrossRef]
11. Sun, M.; Schwingenschlögl, U. δ-CS: A direct-band-gap semiconductor combining auxeticity, ferroelasticity, and potential for high-efficiency solar cells. *Phys. Rev. Appl.* **2020**, *14*, 044015. [CrossRef]
12. Cao, H.; Zhao, Y.; Ho, S.; Seelig, E.; Wang, Q.; Chang, R. Random laser action in semiconductor powder. *Phys. Rev. Lett.* **1999**, *82*, 2278. [CrossRef]
13. Sun, M.; Yan, Y.; Schwingenschlogl, U. Beryllene: A promising anode material for Na-and K-ion batteries with ultrafast charge/discharge and high specific capacity. *J. Phys. Chem. Lett.* **2020**, *11*, 9051–9056. [CrossRef]
14. Bai, K.; Cui, Z.; Li, E.; Ding, Y.; Zheng, J.; Liu, C.; Zheng, Y. Electronic and optical characteristics of GaS/g-C_3N_4 van der Waals heterostructures: Effects of biaxial strain and vertical electric field. *Vacuum* **2020**, *180*, 109562. [CrossRef]
15. Claeyssens, F.; Freeman, C.L.; Allan, N.L.; Sun, Y.; Ashfold, M.N.; Harding, J.H. Growth of ZnO thin films-experiment and theory. *J. Mater. Chem.* **2005**, *15*, 139–148. [CrossRef]
16. Sahoo, T.; Nayak, S.K.; Chelliah, P.; Rath, M.K.; Parida, B. Observations of two-dimensional monolayer zinc oxide. *Mater. Res. Bull.* **2016**, *75*, 134–138. [CrossRef]
17. Altuntasoglu, O.; Matsuda, Y.; Ida, S.; Matsumoto, Y. Syntheses of zinc oxide and zinc hydroxide single nanosheets. *Chem. Mater.* **2010**, *22*, 3158–3164. [CrossRef]
18. Qin, W.; Yuan, Z.; Gao, H.; Zhang, R.; Meng, F. Perovskite-structured $LaCoO_3$ modified ZnO gas sensor and investigation on its gas sensing mechanism by first principle. *Sendor. Actuat. B-Cheim.* **2021**, *341*, 130015. [CrossRef]
19. Shen, Y.; Yuan, Z.; Cheng, F.; Cui, Z.; Ma, D.; Bai, Y.; Zhao, S.; Deng, J.; Li, E. Preparation and characterization of ZnO/graphene/graphene oxide/multi-walled carbon nanotube composite aerogels. *Front. Chem.* **2022**, *10*, 992482. [CrossRef]
20. Shishiyanu, S.T.; Shishiyanu, T.S.; Lupan, O.I. Sensing characteristics of tin-doped ZnO thin films as NO_2 gas sensor. *Sendor. Actuat. B-Cheim.* **2005**, *107*, 379–386. [CrossRef]
21. Cui, Z.; Bai, K.; Ding, Y.; Wang, X.; Li, E.; Zheng, J.; Wang, S. Electronic and optical properties of janus MoSSe and ZnO vdWs heterostructures. *Superlattices Microstruct.* **2020**, *140*, 106445. [CrossRef]
22. Wang, S.; Ren, C.; Tian, H.; Yu, J.; Sun, M. MoS_2/ZnO van der Waals heterostructure as a high-efficiency water splitting photocatalyst: A first-principles study. *Phys. Chem. Chem. Phys.* **2018**, *20*, 13394–13399. [CrossRef] [PubMed]
23. Shen, Y.; Yuan, Z.; Cui, Z.; Ma, D.; Yuan, P.; Yang, K.; Dong, Y.; Wang, F.; Li, E. The Electronic Properties of g−ZnO Modulated by Organic Molecules Adsorption. *Crystals* **2022**, *12*, 882. [CrossRef]
24. Guo, H.; Zhao, Y.; Lu, N.; Kan, E.; Zeng, X.C.; Wu, X.; Yang, J. Tunable magnetism in a nonmetal-substituted ZnO monolayer: A first-principles study. *J. Phys. Chem. C* **2012**, *116*, 11336–11342. [CrossRef]
25. Cui, Z.; Yang, K.; Shen, Y.; Yuan, Z.; Dong, Y.; Yuan, P.; Li, E. Toxic gas molecules adsorbed on intrinsic and defective WS_2: Gas sensing and detection. *Appl. Surf. Sci.* **2023**, *613*, 155978. [CrossRef]
26. Kresse, G.; Furthmüller, J. Efficiency of ab-initio total energy calculations for metals and semiconductors using a plane-wave basis set. *Comp. Mater. Sci* **1996**, *6*, 15–50. [CrossRef]
27. Perdew, J.P.; Burke, K.; Ernzerhof, M. Generalized gradient approximation made simple. *Phys. Rev. Lett.* **1996**, *77*, 3865. [CrossRef]
28. Kresse, G.; Joubert, D. From ultrasoft pseudopotentials to the projector augmented-wave method. *Phys. Rev. B* **1999**, *59*, 1758. [CrossRef]
29. Grimme, S.; Antony, J.; Ehrlich, S.; Krieg, H. A consistent and accurate ab initio parametrization of density functional dispersion correction (DFT-D) for the 94 elements H-Pu. *J. Chem. Phys.* **2010**, *132*, 154104. [CrossRef]
30. Zhang, L.; Cui, Z. Electronic, Magnetic, and Optical Performances of Non-Metals Doped Silicon Carbide. *Front. Chem.* **2022**, *10*. [CrossRef]

31. Zhang, L.; Cui, Z. Theoretical Study on Electronic, Magnetic and Optical Properties of Non-Metal Atoms Adsorbed onto Germanium Carbide. *Nanomaterials* **2022**, *12*, 1712. [CrossRef]
32. Cui, Z.; Wu, H.; Bai, K.; Chen, X.; Li, E.; Shen, Y.; Wang, M. Fabrication of a g-C_3N_4/MoS_2 photocatalyst for enhanced RhB degradation. *Phys. E Low-Dimens. Syst. Nanostruct.* **2022**, *144*, 115361. [CrossRef]
33. Sun, M.; Re Fiorentin, M.; Schwingenschlögl, U.; Palummo, M. Excitons and light-emission in semiconducting $MoSi_2X_4$ two-dimensional materials. *npj 2D Mater. Appl.* **2022**, *6*, 81. [CrossRef]
34. Wang, V.; Xu, N.; Liu, J.; Tang, G.; Geng, W.T. VASPKIT: A user-friendly interface facilitating high-throughput computing and analysis using VASP code. *Comput. Phys. Commun.* **2021**, *267*, 108033. [CrossRef]
35. Yang, K.; Cui, Z.; Li, E.; Ma, D.; Shen, Y.; Yuan, Z.; Dong, Y. Tuning electronic behaviors of WS_2 by molecular doping. *Mater. Today Commun.* **2022**, *33*, 104226. [CrossRef]
36. Sun, M.; Luo, Y.; Yan, Y.; Schwingenschlögl, U. Ultrahigh Carrier Mobility in the Two-Dimensional Semiconductors B_8Si_4, B_8Ge_4, and B_8Sn_4. *Chem. Mater.* **2021**, *33*, 6475–6483. [CrossRef]
37. Cui, Z.; Luo, Y.; Yu, J.; Xu, Y. Tuning the electronic properties of $MoSi_2N_4$ by molecular doping: A first principles investigation. *Phys. E Low-Dimens. Syst. Nanostruct.* **2021**, *134*, 114873. [CrossRef]
38. Cui, Z.; Wang, X.; Ding, Y.; Li, E.; Bai, K.; Zheng, J.; Liu, T. Adsorption of CO, NH_3, NO, and NO_2 on pristine and defective g-GaN: Improved gas sensing and functionalization. *Appl. Surf. Sci.* **2020**, *530*, 147275. [CrossRef]
39. Cui, Z.; Zhang, S.; Wang, L.; Yang, K. Optoelectronic and magnetic properties of transition metals adsorbed Pd_2Se_3 monolayer. *Micro Nanostruct.* **2022**, *167*, 207260. [CrossRef]
40. Cui, Z.; Yang, K.; Ren, K.; Zhang, S.; Wang, L. Adsorption of metal atoms on $MoSi_2N_4$ monolayer: A first principles study. *Mater. Sci. Semicond. Process.* **2022**, *152*, 107072. [CrossRef]
41. Chen, H.; Qu, Y.; Ding, J.; Fu, H. Adsorption behavior of graphene-like ZnO monolayer with oxygen vacancy defects for NO_2: A DFT study. *Superlattices Microstruct.* **2019**, *134*, 106223. [CrossRef]
42. Sun, Y.; Wang, H. The electronic properties of native interstitials in ZnO. *Phys. B* **2003**, *325*, 157–163. [CrossRef]
43. Huang, B.; Zhou, T.; Wu, D.; Zhang, Z.; Li, B. Properties of vacancies and N-doping in monolayer g−ZnO: First-principles calculation and molecular orbital theory analysis. *Acta Phys. Sin.* **2019**, *68*, 246301. [CrossRef]
44. Zhang, Z.; Zhou, T.; Zhao, H.; Wei, X. First-principles calculations of 5d atoms doped hexagonal-AlN sheets: Geometry, magnetic property and the influence of symmetry and symmetry-breaking on the electronic structure. *Chin. Physic. B* **2013**, *23*, 016801. [CrossRef]
45. QingYu, H.; Yong, L.; ChunWang, Z. First-principles study of Al-doped and vacancy on the magnetism of ZnO. *Acta Phys. Sin.* **2017**, *66*, 067202.
46. Safari, F.; Moradinasab, M.; Fathipour, M.; Kosina, H. Adsorption of the NH_3, NO, NO_2, CO_2, and CO gas molecules on blue phosphorene: A first-principles study. *Appl. Surf. Sci.* **2019**, *464*, 153–161. [CrossRef]
47. Li, Q.; Liu, Y.; Chen, D.; Miao, J.; Zhi, X.; Deng, S.; Lin, S.; Jin, H.; Cui, D. Nitrogen Dioxide Gas Sensor Based on Ag-Doped Graphene: A First-Principle Study. *Chemosensors* **2021**, *9*, 227. [CrossRef]
48. Ruccolo, S.; Sattler, W.; Rong, Y.; Parkin, G. Modulation of Zn-C bond lengths induced by ligand architecture in zinc carbatrane compounds. *J. Am. Chem. Soc.* **2016**, *138*, 14542–14545. [CrossRef]
49. Bosi, F.; Andreozzi, G.B.; Hålenius, U.; Skogby, H. Zn-O tetrahedral bond length variations in normal spinel oxides. *Am. Mineral.* **2011**, *96*, 594–598. [CrossRef]
50. Halfen, J.A.; Mahapatra, S.; Wilkinson, E.C.; Kaderli, S.; Young, V.G., Jr.; Que, L., Jr.; Zuberbühler, A.D.; Tolman, W.B. Reversible cleavage and formation of the dioxygen O-O bond within a dicopper complex. *Science* **1996**, *271*, 1397–1400. [CrossRef]
51. Modec, B. Crystal chemistry of zinc quinaldinate complexes with pyridine-based ligands. *Crystals* **2018**, *8*, 52. [CrossRef]
52. Fang, H.; Banjade, H.; Jena, P. Realization of the Zn^{3+} oxidation state. *Nanoscale* **2021**, *13*, 14041–14048. [CrossRef]
53. Demaison, J.; Császár, A.G. Equilibrium CO bond lengths. *J. Mol. Struct.* **2012**, *1023*, 7–14. [CrossRef]
54. Hu, W.; Li, Z.; Yang, J. Electronic and optical properties of graphene and graphitic ZnO nanocomposite structures. *J. Chem. Phys.* **2013**, *138*, 124706. [CrossRef]
55. Zhou, C.; Yang, W.; Zhu, H. Mechanism of charge transfer and its impacts on Fermi-level pinning for gas molecules adsorbed on monolayer WS_2. *J. Chem. Phys.* **2015**, *142*, 214704. [CrossRef]
56. Salih, E.; Ayesh, A.I. First principle study of transition metals codoped MoS_2 as a gas sensor for the detection of NO and NO_2 gases. *Phys. E Low-Dimens. Syst. Nanostruct.* **2021**, *131*, 114736. [CrossRef]
57. Wang, S.; Yu, J. Magnetic Behaviors of 3d Transition Metal-Doped Silicane: A First-Principle Study. *J. Supercond. Novel Magn.* **2018**, *31*, 2789–2795. [CrossRef]